Optics Letters

Coherent injection of light into an absorbing scattering medium with a microscopic pore

Alexey G. Yamilov,[1,*] Raktim Sarma,[2] Vladislav V. Yakovlev,[3] and Hui Cao[2,4]

[1]Physics Department, Missouri University of Science and Technology, Rolla, Missouri 65409, USA
[2]Department of Applied Physics, Yale University, New Haven, Connecticut 06520, USA
[3]Department of Biomedical Engineering, Texas A&M University, College Station, Texas 77843, USA
[4]e-mail: hui.cao@yale.edu
*Corresponding author: yamilov@mst.edu

Received 31 January 2018; accepted 27 March 2018; posted 5 April 2018 (Doc. ID 320959); published 1 May 2018

We demonstrate that interplay between absorption and scattering in a dielectric medium with a microscopic pore gives rise to eigenchannels concentrated in the pore. Such a circumvention of attenuation leads to high transmission. By exciting such eigenchannels in a disordered nanophotonic system with a wavefront shaping technique, we experimentally confirm enhanced injection at depths exceeding the limiting length scales set by scattering, absorption, and diffraction.

OCIS codes: (110.7050) Turbid media; (030.1670) Coherent optical effects; (110.7348) Wavefront encoding.

https://doi.org/10.1364/OL.43.002189

Delivery of a sufficient dose of electromagnetic radiation into a strongly scattering medium is the foremost condition for a wide range of sensing, imaging, therapeutic, and other applications. This goal is hampered by turbidity in the system—light propagation proceeds via a diffusion process, which leads to strong suppression of light intensity at distances greater than transport mean free path ℓ away from the source [1].

Tailoring the incident fields via a wavefront shaping technique [2,3] offers an exciting approach to enhance light delivery by exploiting the so-called open eigenchannels [4–8] that penetrate, even through a scattering medium of thickness much larger than transport mean free path. The efficacy of the open eigenchannels is limited by absorption that leads to extinction on the scales larger than $\xi_a = \sqrt{Dt_a}$ [9], Fig. 1(a), where D is the diffusion coefficient, and t_a is the ballistic absorption time.

Recently, a different approach to light delivery into turbid media has been proposed [10–12]. It is based on modification of the surface of a scattering medium by creating a small conically shaped hole of area A, via, e.g., laser ablation, to inject the light directly into the hole by focusing; see Fig. 1(b). This technique turned out to be highly efficient in enhancing light-matter interactions [11,12] because the light is unlikely to escape through the same pore after the diffusion process has been initiated deep (at multiple ℓ's) inside the medium. Diffraction of light in the pore limits injection to distances smaller than $L_{\text{diffr}} \sim A/\lambda$, where A is the area of the opening, and λ is the wavelength of the electromagnetic radiation.

Microscopic pores can readily exist in many natural and artificial materials [13] such as polymers [14], weathered natural stone, or building materials [15]; stress-fractured paint/surface coatings; and follicular and other pores in skin [16]. However, for narrow pores, L_{diffr} might become comparable to the transport mean free path, making diffraction the limiting factor for the injection depth.

In this Letter, we demonstrate the existence of penetrating quasi-open eigenchannels in an absorbing scattering medium with a microscopic pore. They are concentrated in the region of the pore, thus circumventing scattering (ℓ), absorption (ξ_a), and diffraction (L_{diffr}) constraints for injection depth; see Fig. 1(c). Using wavefront shaping to coherently excite quasi-open channels and imaging light intensity distribution inside the planar disordered nanophotonic waveguide, we experimentally confirm an efficient injection of light into scattering medium via a narrow pore.

We begin by performing numerical simulations in systems that will have direct correspondence with planar disordered photonic nanostructures studied experimentally below. We consider a two-dimensional (2D) waveguide of length L and width W filled with scattering medium characterized by the

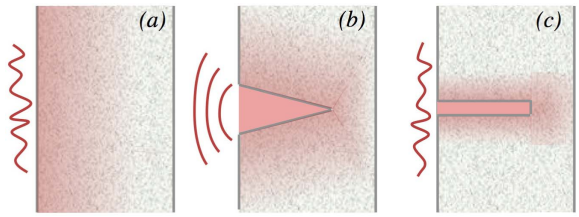

Fig. 1. (a) Enhancing light penetration into an absorbing scattering medium by tailoring the incident wavefront to excite a high-transmission eigenchannel of the system. (b) Focusing light into an artificially created conically shaped hole. (c) Coupling light into a quasi-open eigenchannel concentrated in a narrow micro-pore by wavefront shaping, allowing injection to the depths exceeding the transport mean free path, absorption, and diffraction length scales.

transport mean free path ℓ; see Fig. 2(a). The choice of geometry is motivated by our ability to experimentally verify light propagation in 2D structures, while the extension to 3D [11,12] is relatively straightforward. Reflecting boundary conditions are applied at $y = \pm W/2$; the boundaries are open at $x = 0, L$, and the wave is incident from the left. The system is in the regime of a diffusive transport [17] with $\lambda \ll \ell \ll W, L$ and the dimensionless conductance $g_p = (\pi/2)N\ell/L \gg 1$, where $N = W/(\lambda/2) \gg 1$ is the number of waveguide modes. The system also meets the condition of strong absorption $\xi_a < L$, while still avoiding over-damping, i.e., $\ell \ll \xi_a$. When introducing the pore of width W_{pore}, aside from $\lambda, \ell < W_{\text{pore}} < W$ conditions, we also set the additional condition $L_{\text{diffr}} < L$. The latter will allow us to test whether it is possible to overcome the diffraction limit for light injection. In 2D systems where $L_{\text{diffr}} \simeq W_{\text{pore}}^2/2\lambda$, imposing this additional requirement leads to $W_{\text{pore}} < (2L\lambda)^{1/2}$.

Meeting all stated conditions, particularly in an experiment, requires meticulous adjustment of system parameters. In that regard, we normalize the length scales in our numerical simulations to match those in the experimental system below. Specifically, we chose $\ell = 2.2$ μm, $\xi_a = 30$ μm, $L = 80$ μm, $W = 30$ μm, $W_{\text{pore}} = 7.5$ μm, $L_{\text{diffr}} \simeq 50$ μm and the wavelength in the medium $\lambda = 0.53$ μm. Such a choice meets all the criteria defined above, specifically, $\ell, \xi_a, L_{\text{diffr}} < L$. The numerical simulations are based on the recursive Green function method [18], allowing us to compute the transmission matrix $\hat{t}$, as well as the field distribution throughout the volume of the system; see Refs. [8,19,20].

As a reference, we consider the case with unoptimized excitation—constant flux is incident through all input waveguide modes. Figure 2(a) shows computed intensity $\langle I(x,y)\rangle$ averaged over an ensemble of 1000 realizations of disorder in the sample without pore. As expected, the cross section averaged intensity $\langle I(x)\rangle$, the solid line in Fig. 2(i), shows exponential decay because $\xi_a < L$. To find transmission eigenchannels, we perform singular value decomposition of the transmission matrix [3,5,21,22] $\hat{t} = \hat{U}\hat{\tau}^{1/2}\hat{V}^{\dagger}$, where $\hat{\tau}$ is the diagonal matrix of the transmission eigenvalues, and $\hat{U}$, $\hat{V}$ are unitary matrices. Coupling to the eigenchannel with the maximum eigenvalue τ_1 can be accomplished by injecting light with complex amplitude given by the corresponding left-singular vector V_{i1}. Unlike passive systems where there exist open eigenchannels with $\tau_1 \simeq 1$ [23,24], in absorbing systems, the maximum transmission eigenvalue is less than one [9,19]. We will refer to such an eigenchannel as the maximum transmission eigenchannel; see Fig. 2(e). $\langle I(x)\rangle$ in Fig. 2(i) shows that, unlike passive systems, the peak intensity is located at $x \sim \xi_a < L/2$. Deeper into the system, the intensity is expected to transition to exponential decay due to absorption.

Under unoptimized excitation, a sample with a pore of size $W_{\text{pore}} = 7.5$ μm and $L_{\text{pore}} = 78$ μm; see Fig. 2(b), shows a slower decay with depth x compared to panel (a). This is because the pore region does not lead to scattering or absorption, causing the cross section averaged intensity to exhibit a diminished attenuation. However, we do not observe a significant concentration of intensity in the region of the pore; see also Fig. 2(d). In contrast, when coupling to the quasi-open eigenchannel, Fig. 2(f), the intensity is confined to the region of the pore leading to 85% transmission. This compares to 6.5% in the unoptimized case—Fig. 2(b)—and 36% for the maximum transmission eigenchannel in system without a pore—Fig. 2(e).

Maximum transmission eigenchannels have been observed to exhibit a tendency to minimize absorption via more ballistic (straight path) propagation [25] in systems with spatially uniform absorption or to avoid regions with locally elevated absorption [26,27]. The case of an absorbing scattering medium with a microscopic pore considered in this Letter may be viewed as the extreme example of such an avoidance. To investigate this possibility, we performed numerical simulations in the equivalent system without absorption; Fig. 2(g). Although

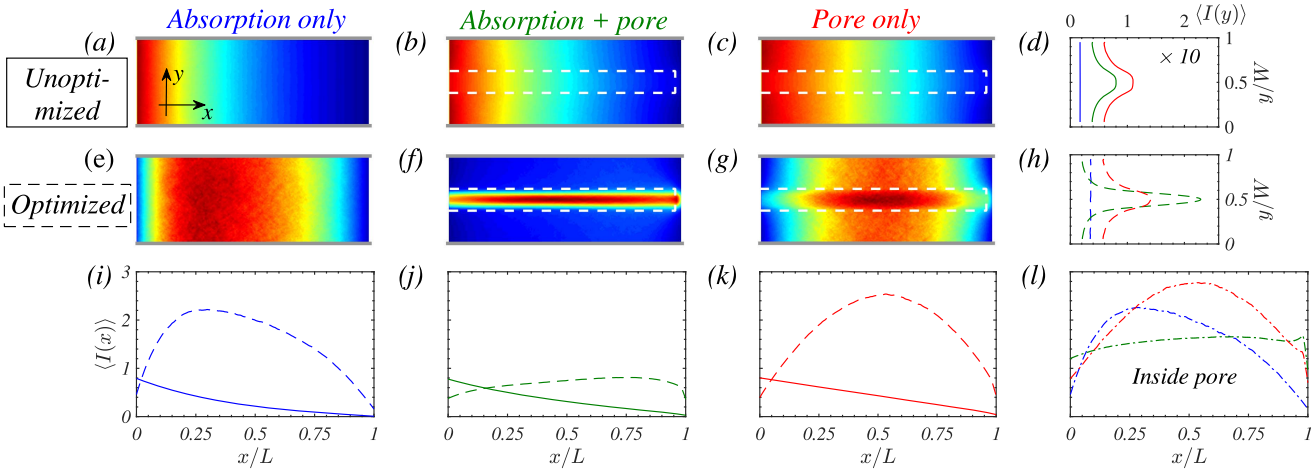

Fig. 2. Numerical simulations of light propagation in scattering systems with and without absorption or micro-pores. The outline of the pore is shown by a white dashed line. The unoptimized excitation (first row) and excitation of the highest transmission eigenchannel (second row) are compared. The first column depicts the ensemble-averaged intensity in the disordered waveguide with absorption but no pore; a loss-less pore is introduced in the second column; and a loss-less system with a pore is considered in the third column. A quasi-open eigenchannel is strongly confined in the pore only in the absorbing system, panel (f). Panels (d) and (h) plot the intensity close to the output end of the system. Panels (i)–(k) plot the depth dependence of the cross section averaged intensity for three systems with unoptimized (solid lines) and optimized (dashed lines) excitations. Panel (l) depicts the depth dependence of the intensity averaged only over the region of the pore.

the maximum transmission eigenchannel exhibits an increased intensity in the pore, which is void of scattering, the intensity outside the pore is of a comparable value. Unlike the absorbing case where the maximum transmission eigenvalues are grouped in a separate peak (the green curve in Fig. 3), the distribution of the transmission eigenvalues in a passive system (red line) is the universal bimodal distribution [23,28], allowing co-existence of the transversely confined and extended eigenchannels. Statistical averaging over the two types of eigenchannels could conceivably give an intensity pattern in Fig. 2(g).

An important question arises as to whether absorption leads to the *formation* of the quasi-open eigenchannel confined in the pore or merely promotes the *selection* of the confined eigenchannel from a group of open eigenchannels of the passive system, some of which are delocalized in the transverse direction. By performing the detailed analysis of spatial profiles of all highly transmitting eigenchannels with $\tau \sim 1$, we could not identify distinct confined/delocalized classes. The inset in Fig. 3 shows a scatter plot of a measure of transverse localization f versus τ for the most confined eigenchannel in each disorder configuration with (green symbols) and without (red symbols) absorption. f is defined as a ratio between the normalized intensity $I(x,y)/\int_{-W/2}^{W/2} I(x,y)\mathrm{d}y$ averaged over the width of the pore to its average value over the entire cross section, whereas open eigenchannels of the passive system exhibit varying, but only moderate degree of concentration in the region of the pore, quasi-open eigenchannels of the absorbing system are strongly confined in the pore with a narrow distribution of f around 2.3. Furthermore, higher values of f correlate with higher transmission eigenvalues τ. Therefore, we conclude that an *interplay between scattering and absorption* [26,27] *leads to the formation* of the quasi-open eigenchannel concentrated in the pore of the absorbing system, Fig. 2(f), and forming a distinct peak in the density of the transmission eigenvalues; see the shaded region in Fig. 3.

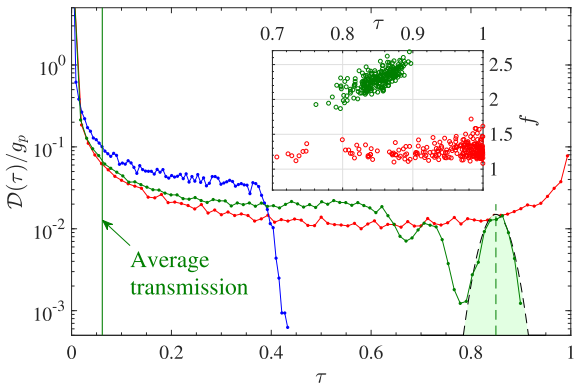

Fig. 3. Density of transmission eigenvalues in three systems depicted in Figs. 2(a)–2(c) using the same color schemes. In each case, the density is normalized by the value of dimensionless conductance g_p for the corresponding passive system. The maximum transmission eigenvalue in the absorbing scattering system with a micro-pore (green line) forms a distinct peak (shaded Gaussian peak), centered at 0.85 (dashed vertical line). The area of the shaded region corresponds to having one eigenchannel per disorder realization. The inset is a scatter plot of transverse intensity confinement f versus the transmission eigenvalue τ for the most confined eigenchannel in 250 different disordered samples with (green) and without (red) absorption.

To demonstrate experimentally the efficient injection of light through a micro-pore via a quasi-open eigenchannel, we fabricated a planar scattering waveguide in a silicon (220 nm thick) on insulator (3 μm oxide layer) wafer shown in Fig. 4(a). The reflecting boundaries are achieved via photonic crystal with an in-plane bandgap due to the triangular arrangement of air holes (diameter 360 nm, lattice constant 505 nm) at the operating vacuum wavelength $\lambda_0 = 1.51$ μm; see the left inset in Fig. 4(a). Scattering is achieved by an array of randomly positioned holes of diameter 90 nm and filling density 6%, fabricated by an inductively coupled-plasma reactive-ion etching. These parameters were chosen to obtain the desired transport mean free path and absorption length, as quoted in the numerical simulations above. The out-of-plane scattering, rather than material absorption, is responsible for loss described by ξ_a [29]. This loss is the basis for imaging into the system because it is proportional to the light intensity remaining in the waveguide.

Omitting scatterers allows introducing a non-scattering region of the pore. The absence of loss due the lack of scattering in the micro-pore also prevents us from detecting the light

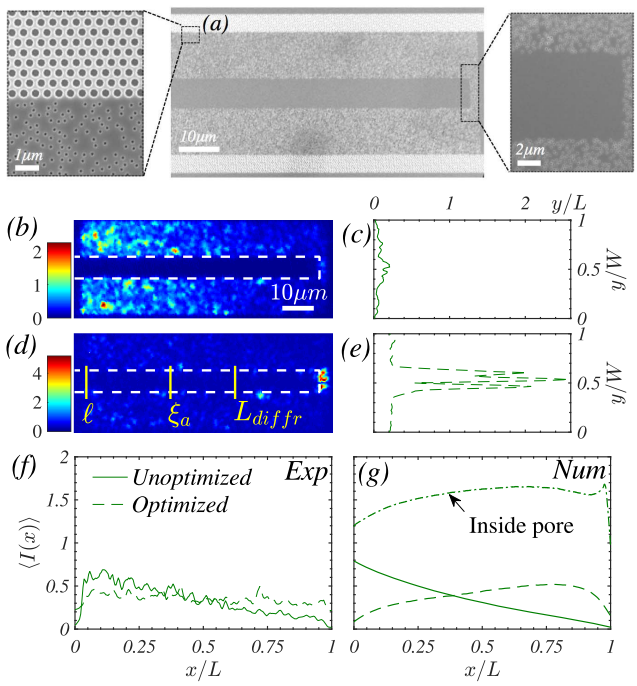

Fig. 4. (a) Top-view scanning electron micrograph of the fabricated disordered waveguide. The scattering is due to randomly positioned holes. The sidewalls of the waveguide are made of a triangular lattice of air holes that supports an in-plane photonic bandgap and acts as a reflecting boundary (the left inset). The pore is terminated with a thin layer of a scattering medium (the right inset). (b)–(f) Experimentally measured 2D intensity distribution inside the waveguide. The unoptimized input (b), (c) and optimized input (d), (e) are compared. This process of optimization causes preferential excitation of quasi-open eigenchannels. Panel (d) shows the characteristic scattering/absorption/diffraction scales defined in the text. The white box marks the boundaries of the "pore"—the non-scattering region where light intensity cannot be imaged from the top. Depth dependence of intensity averaged over (f) the outside of the pore agrees well with (g) the numerics. For comparison, (g) also shows the intensity profile inside the pore (dashed–dotted line). The intensity profiles at the output (c) and (e) also agree with those in numerical simulations Figs. 2(d) and 2(h).

intensity there directly. To circumvent this constraint, we added a 2 μm scattering region at the end of the pore that scatters transmitted light. The parameters of the experimental system in Fig. 4 match those used in the simulation above. Lastly, the ensemble averaging is obtained by averaging over several wavelengths detuned slightly from the center wavelength λ_0.

Figure 4(b) shows measured intensity for the case of an unoptimized incident field; it directly correspond to the numerical simulations depicted in Fig. 2(b). Unlike the simulations, in the experiment, it is not possible to directly image light intensity inside the micro-pore because light does not scatter out of the plane of the waveguide there. Plotting the intensity averaged over a cross section of the waveguide, excluding the section of the pore, we see a monotonous decay, Fig. 4(f), in agreement with Fig. 2(j).

To excite a quasi-open eigenchannel, we employ the wavefront shaping procedure for controlling the incident field, similar to that in Refs. [8,27]. The phases of the individual pixels in the spatial light modulator were optimized via a sequential algorithm [30]. The cost function was chosen to be the ratio between the cross section averaged intensity at the end and front of the disordered waveguide. Maximizing this function yields preferential excitation of the quasi-open eigenchannel [8]. The distribution of the transmission eigenvalues in Fig. 3 has a distinct peak associated with the quasi-open eigenchannel. Furthermore, the numerical simulations suggest that the quasi-open eigenchannel should be present in every disorder realization, because the shaded area in Fig. 3 is equal to the number of realizations. This is important from the experimental standpoint, since the number of experimental measurements at detuned wavelengths (statistical ensemble) is relatively small.

Figure 4(d) shows the intensity distribution after performing phase optimization of the incident wavefront. The transverse intensity close to the output surface of the disordered waveguide, Fig. 4(e), shows a strong concentration of intensity in the micro-pore, in agreement with the profile of the quasi-open eigenchannel found in simulation Fig. 2(h). The depth profile, shown as a dashed line in Fig. 4(f), is extended throughout the system as in simulations, panel (g). A slight difference between the two is due to the excitation of additional high transmission channels in the optimization scheme.

In conclusion, we used numerical simulations to demonstrate that a scattering absorbing system with a micro-pore can support eigenchannels that minimize absorption and scattering by concentrating the intensity inside the pore. This coherent effect arises due to an intricate interplay between the scattering and absorption in the regime $L > L_{\mathrm{diffr}}$, making it challenging for semi-classical treatments as in, e.g., Ref. [31]. Coupling to these quasi-open eigenchannels can be accomplished by a left-singular vector of the complex transmission matrix or via optimization of the incident wavefront with a cost function that selects highly transmitting channels. We employed the second strategy to experimentally confirm the possibility of enhanced penetration. Specifically, we designed a 2D disordered nanophotonic system where intensity can be measured inside the medium. We demonstrated the light injection to the depths exceeding all limiting length scales: (1) the transport mean free path, (2) the absorption length associated with the diffusive process in lossy media, and (3) the diffraction length that limits the depth of the ballistic injection through an aperture; see Fig. 4(d). The method of delivering light deep into a turbid medium can offer a new avenue for enhancing light-matter interactions with applications in sensing and imaging [32,33].

Funding. Directorate for Mathematical and Physical Sciences (MPS) (DMR-1205223, DMR-1205307); Office of Naval Research (ONR) (N00014-13-1-0649); Directorate for Engineering (ENG) (ECCS-1509268); Air Force Office of Scientific Research (AFOSR) (FA9550-15-1-0517).

REFERENCES

1. L. V. Wang and H. Wu, *Biomedical Optics: Principles and Imaging* (Wiley-Interscience, 2007).
2. P. A. Mosk, A. Lagendijk, G. Lerosey, and M. Fink, Nat. Photonics **6**, 283 (2012).
3. S. Rotter and S. Gigan, Rev. Mod. Phys. **89**, 015005 (2017).
4. W. Choi, A. P. Mosk, Q. H. Park, and W. Choi, Phys. Rev. B **83**, 134207 (2011).
5. B. Gérardin, J. Laurent, A. Derode, C. Prada, and A. Aubry, Phys. Rev. Lett. **113**, 173901 (2014).
6. M. Davy, Z. Shi, J. Park, C. Tian, and A. Z. Genack, Nat. Commun. **6**, 6893 (2015).
7. O. S. Ojambati, H. Yilmaz, A. Lagendijk, A. P. Mosk, and W. L. Vos, New J. Phys. **18**, 043032 (2016).
8. R. Sarma, A. Yamilov, S. Petrenko, Y. Bromberg, and H. Cao, Phys. Rev. Lett. **117**, 086803 (2016).
9. P. W. Brouwer, Phys. Rev. B **57**, 10526 (1998).
10. V. N. Lednev, P. A. Sdvizhenskii, M. Y. Grishin, M. N. Filippov, A. N. Shchegolikhin, and S. M. Pershin, Opt. Lett. **42**, 607 (2017).
11. J. V. Thompson, B. H. Hokr, W. Kim, C. W. Ballmann, B. Applegate, J. Jo, A. Yamilov, H. Cao, M. O. Scully, and V. V. Yakovlev, Proc. Natl. Acad. Sci. USA **114**, 7941 (2017).
12. J. V. Thompson, B. H. Hokr, W. Kim, C. W. Ballmann, B. Applegate, J. Jo, A. Yamilov, H. Cao, M. O. Scully, and V. V. Yakovlev, Appl. Phys. Lett. **111**, 201105 (2017).
13. U. G. K. Wegst, H. Bai, E. Saiz, A. P. Tomsia, and R. O. Ritchie, Nat. Mater. **14**, 23 (2014).
14. H. Zhang, I. Hussain, M. Brust, M. F. Butler, S. P. Rannard, and A. I. Cooper, Nat. Mater. **4**, 787 (2005).
15. L. M. Anovitz and D. R. Cole, Rev. Mineral. Geochem. **80**, 61 (2015).
16. F. Flament, G. Francois, H. Qiu, C. Ye, T. Hanaya, D. Batisse, S. Cointereau-Chardon, M. Seixas, S. E. D. Belo, and R. Bazin, Clin. Cosmet. Invest. Dermatol. **8**, 85 (2015).
17. M. C. van Rossum and T. M. Nieuwenhuizen, Rev. Mod. Phys. **71**, 313 (1999).
18. C. W. Groth, M. Wimmer, A. R. Akhmerov, and X. Waintal, New J. Phys. **16**, 063065 (2014).
19. A. Yamilov, S. Petrenko, R. Sarma, and H. Cao, Phys. Rev. B **93**, 100201 (2016).
20. M. Koirala, R. Sarma, H. Cao, and A. Yamilov, Phys. Rev. B **96**, 054209 (2017).
21. S. M. Popoff, G. Lerosey, R. Carminati, M. Fink, A. C. Boccara, and S. Gigan, Phys. Rev. Lett. **104**, 100601 (2010).
22. J. Yoon, K. Lee, J. Park, and Y. K. Park, Opt. Express **23**, 10158 (2015).
23. O. N. Dorokhov, Solid State Commun. **51**, 381 (1984).
24. Y. Imry, Europhys. Lett. **1**, 249 (1986).
25. S. F. Liew, S. M. Popoff, A. P. Mosk, W. L. Vos, and H. Cao, Phys. Rev. B **89**, 224202 (2014).
26. S. F. Liew and H. Cao, Opt. Express **23**, 11043 (2015).
27. R. Sarma, A. Yamilov, and H. Cao, Appl. Phys. Lett. **110**, 021103 (2017).
28. Y. V. Nazarov, Phys. Rev. Lett. **73**, 134 (1994).
29. A. G. Yamilov, R. Sarma, B. Redding, B. Payne, H. Noh, and H. Cao, Phys. Rev. Lett. **112**, 023904 (2014).
30. I. M. Vellekoop, Opt. Express **23**, 12189 (2015).
31. P. Jacquod and E. V. Sukhorukov, Phys. Rev. Lett. **92**, 116801 (2004).
32. R. Arora, G. I. Petrov, V. V. Yakovlev, and M. O. Scully, Proc. Natl. Acad. Sci. USA **109**, 1151 (2012).
33. R. Arora, G. I. Petrov, V. V. Yakovlev, and M. O. Scully, Anal. Chem. **86**, 1445 (2014).